Hepta- and Octacoordinate Boron in Molecular Wheels of Eight- and Nine-Atom Boron Clusters: Observation and Confirmation**

*Hua-Jin Zhai, Anastassia N. Alexandrova,
K. Alexander Birch, Alexander I. Boldyrev, and Lai-
Sheng Wang**

Clusters of atoms can adopt different atomic arrangements from bulk materials. They often exhibit novel structures and properties, which provide opportunities for new types of chemical bonding and stoichiometry. Herein we report experimental and theoretical evidence that 8- and 9-atom boron clusters are perfectly planar molecular wheels, with a hepta- or octacoordinated central boron atom, respectively, despite the predominance of three-dimensional structures normally found in bulk boron and its compounds.[1–3] Hepta- and octacoordinated planar boron compounds are highly unusual. The radii of the miniature molecular wheels are found to be 1.8 and 2.0 Å for the 8- and 9-atom clusters, respectively. Analyses of their chemical bonding reveal that they possess double (σ and π) aromaticity, which is responsible for the novel molecular structures and the extreme coordination environments.

We produced the B_8^- and B_9^- clusters with a laser vaporization cluster source and probed their electronic structure with photoelectron spectroscopy (PES), analogous to our previous study on the smaller B_5^- and B_6^- clusters.[4,5] Figure 1 shows the PES spectra of B_8^- at three photon energies and those of B_9^- at two photon energies. The 193 nm spectrum of B_8^- revealed four distinct features labeled X, A, B, C (Figure 1b). A fifth band (D) can be tentatively identified, but the signal-to-noise ratios are poor at the
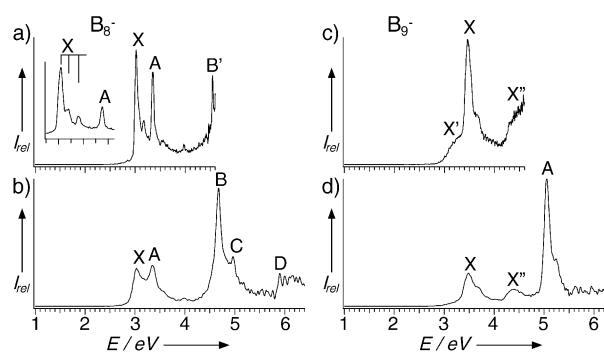
[*] Prof. Dr. L.-S. Wang, Dr. H.-J. Zhai
Department of Physics, Washington State University
2710 University Drive, Richland, WA 99352 (USA)
and
W. R. Wiley Environmental Molecular Sciences Laboratory
Pacific Northwest National Laboratory, MS K8-88
P. O. Box 999, Richland, WA 99352 (USA)
Fax: (+1) 509-376-6066
E-mail: ls.wang@pnl.gov

A. N. Alexandrova, K. A. Birch, Prof. Dr. A. I. Boldyrev
Department of Chemistry and Biochemistry
Utah State University, Logan, UT 84322-0300 (USA)

Figure 1. Photoelectron spectra of a) B_8^- at 266 nm (4.661 eV), the inset shows the spectrum taken at 355 nm (3.496 eV), and b) at 193 nm (6.424 eV). c) The photoelectron spectrum of B_9^- at 266 nm and d) at 193 nm.

high-binding-energy side. At 266 nm (Figure 1a), fine vibrational features were observed for the X band, which were resolved more clearly in the 355 nm spectrum. Two vibrational modes were observed with frequencies of 510 ± 50 and 1160 ± 60 cm^{-1}. A sharp peak (B′), which appeared as a shoulder in the 193 nm spectrum, was also resolved in the 266 nm spectrum of B_8^- (Figure 1a). All the vertical detachment energies (VDEs) are given in Table 1 and compared with theoretical calculations (see below). The sharp peak of the X band in the spectrum of B_8^- defines the electron affinity (EA) of neutral B_8 to be 3.02 ± 0.02 eV.

Table 1: Experimental and theoretical vertical detachment energies in eV for B_8^- and B_9^-.

Observed features	VDE (exp.)[a]	Molecular orbital	Final state	VDE (calcd)[b]	VDE (calcd)[c]
		B_8^- (C_{2v}, $^2B_1$)			
X	3.02(2)	HOMO-1 (1a$_2$)	$^3B_2$	2.99[d]	
A	3.35(2)	HOMO (2b$_1$)	$^1A_1$	3.45[d]	3.41
		HOMO-1 (1a$_2$)	$^1B_2$		3.45
B′	4.55(4)	HOMO-2 (6a$_1$)	$^3B_1$	4.74[d]	
B	4.68(6)	HOMO-3 (4b$_2$)	$^3A_2$	4.78[d]	
		HOMO-3 (4b$_2$)	$^1A_2$		4.79
C	4.98(6)	HOMO-2 (6a$_1$)	$^1B_1$		5.15
		HOMO-4 (1b$_1$)	$^3A_1$	5.86[d]	
		B_9^- (D_{8h}, $^1A_{1g}$)			
X	3.46(6)	HOMO (1e$_{1g}$)	$^2E_{1g}$	3.47[e] (3.38)[e]	
A	5.04(6)	HOMO-1 (2e$_{1u}$)	$^2E_{1u}$	5.07[e] (4.84)[e]	
		HOMO-2 (1a$_{2u}$)	$^2A_{2u}$	(5.78)[e]	

[a] Numbers in parentheses indicate the uncertainties of the last digit. [b] CCSD(T)/6-311+G(2df), [c] EOM-RCCSD(T)/6-311+G(2d) [d] Calculations were done at the RCCSD(T) level of theory. [e] Data in parenthesis are at the ROVGF/6-311+G(2df) level of theory and at the UCCSD(T) level of theory otherwise.

The spectral features of B_9^- (Figure 1c, d) seemed to be broader and are dominated by three main bands (X, X″, A). The weak signals at the low-binding-energy side (X′, Figure 1c) depended on source conditions and could be due to either hot band or isomer contributions. The X″ band around

4.4 eV is very broad and not well defined even under the higher resolution condition at 266 nm (Figure 1 c). The X and A bands are sharper and more intense, each with a short vibrational progression (vibrational spacing ≈1300–1400 cm^{-1}). From the threshold of the X band, we estimated an EA of 3.39 ± 0.06 eV for B_9. The VDEs of the X and A bands are listed in Table 1, and compared with theoretical calculations.

Combining PES and computational chemistry is a powerful means to elucidate the electronic structure and chemical bonding of novel clusters.[6–8] We performed an extensive computational search for the global minimum structures for B_8, B_8^-, B_8^{2-}, B_9, B_9^- by using a hybrid (density functional and Hartree–Fock) method. We found that all five species have planar wheel structures (Figure 2): B_8 and B_8^{2-} are perfect heptagons and B_9^- is a perfect octagon, whereas B_8^- and B_9 have slight in-plane distortions within the heptagonal and octagonal structures, respectively. B_8, B_9, and B_9^- have been calculated previously,[9–13] but there is no consensus among the different studies. Our heptagon triplet structure for B_8 agrees with the theoretical predictions by Bonacic-Koutecky et al.[9] and Boustani.[12] Our octagon structure for B_9^- agrees with a date by Wang and Schleyer.[13]

To confirm our computational results and facilitate comparison with the experimental data, we further calculated the low-lying VDEs for B_8^- and B_9^- using sophisticated ab initio methods (Table 1). To interpret the B_8^- spectra, it is convenient to start from the high symmetry B_8^{2-} structure (Figure 2b). The B_8^{2-} ion is closed-shell and has a degenerate highest occupied molecular orbital (HOMO; $1e_1''$, Figure 3a). Upon one-electron detachment, the resulting doublet B_8^- undergoes a slight Jahn–Teller distortion to C_{2v} symmetry (Figure 2c) with the following valence electron configuration: $1a_1^2 2a_1^2 1b_2^2 2b_2^2 3a_1^2 4a_1^2 3b_2^2 5a_1^2 1b_1^2$-$4b_2^2 6a_1^2 1a_2^2 2b_1^1$. The doubly degenerate $1e_1''$-HOMO is now split into $2b_1$ (HOMO) and $1a_2$ (HOMO-1) in the C_{2v} structure. When a further electron is removed from B_8^-, the final state can be either a singlet (detachment from the singly occupied $2b_1$ MO) or a triplet (detachment from the doubly occupied $1a_2$ MO). The lowest energy peak at 3.02 eV in the B_8^- spectra (Figure 1) corre-
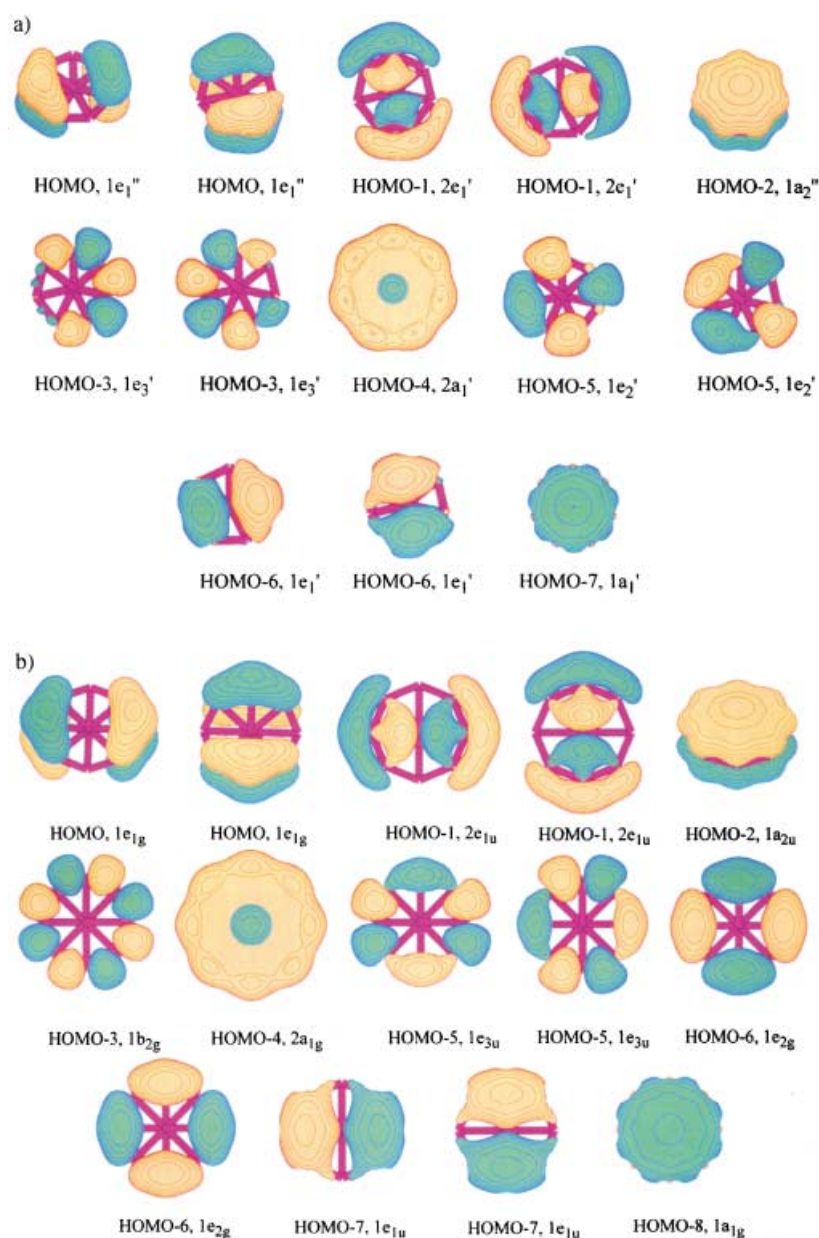

a)

HOMO, $1e_1''$ · HOMO, $1e_1''$ · HOMO-1, $2e_1'$ · HOMO-1, $2e_1'$ · HOMO-2, $1a_2''$

HOMO-3, $1e_3'$ · HOMO-3, $1e_3'$ · HOMO-4, $2a_1'$ · HOMO-5, $1e_2'$ · HOMO-5, $1e_2'$

HOMO-6, $1e_1'$ · HOMO-6, $1e_1'$ · HOMO-7, $1a_1'$

b)

HOMO, $1e_{1g}$ · HOMO, $1e_{1g}$ · HOMO-1, $2e_{1u}$ · HOMO-1, $2e_{1u}$ · HOMO-2, $1a_{2u}$

HOMO-3, $1b_{2g}$ · HOMO-4, $2a_{1g}$ · HOMO-5, $1e_{3u}$ · HOMO-5, $1e_{3u}$ · HOMO-6, $1e_{2g}$

HOMO-6, $1e_{2g}$ · HOMO-7, $1e_{1u}$ · HOMO-7, $1e_{1u}$ · HOMO-8, $1a_{1g}$

Figure 3. Molecular orbital pictures. a) D_{7h} B_8^{2-}, b) D_{8h} B_9^-.

sponds to electron detachment from the $1a_2$ orbital resulting in a triplet state (Table 1), which upon geometry optimization relaxes to the perfect heptagon triplet ground state of B_8
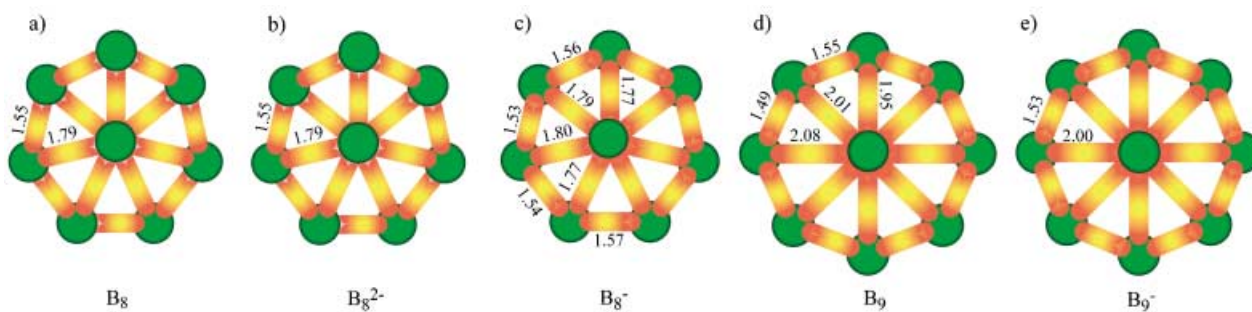

Figure 2. Optimized global minimum structures. a) D_{7h} B_8, b) D_{7h} B_8^{2-}, c) C_{2v} B_8^-, d) D_{2h} B_9, e) D_{8h} B_9^-. Selected bond lengths given in Å.

(Figure 2a). The calculated VDE of 2.99 eV is in excellent agreement with the experimental value of 3.02 eV. According to our calculations two vibrational modes (481 and 1243 cm^{-1}) can be responsible for the C_{2v}–D_{7h} transformation and these frequencies agree well with the experimentally observed frequencies at 510 ± 50 and 1160 ± 60 cm^{-1}.

The second feature A of the B_8^- spectrum is observed at 3.35 eV (Figure 1a), in excellent agreement with the calculated VDE from the $2b_1$ orbital (Table 1). Our calculated VDE for the singlet final state from detachment from the $1a_2$ orbital is nearly degenerate with that of the $2b_1$ orbital and may also contribute to the A band. The next calculated VDE is at 4.74 eV for the triplet final state from detachment from the $6a_1$ orbital (HOMO-2), which is assigned to the B′ band at 4.55 eV (Table 1). Two other detachment channels, the triplet and singlet final states from the $4b_2$ orbital (HOMO-3), have VDEs very close to each other and are assigned to the intense B band at 4.68 eV. The triplet final state from the $6a_1$ orbital has a calculated VDE of 5.15 eV and is assigned to the C band at 4.98 eV. There are no single-electron detachment channels between 3.4 and 4.7 eV. This calculated spectral pattern is in excellent agreement with the PES spectra of B_8^- (Figure 1a, b). The weak feature around 4 eV in the PES spectra is likely to be due to a two-electron transition. The next calculated VDE is at 5.86 eV from HOMO-4 ($1b_1$). Although the signal-to-noise ratio is poor in the high-binding-energy side of the B_8^- spectrum (Figure 1b), we can tentatively identify a detachment feature (D) around 5.9 eV. The overall agreement between the calculated VDEs and the PES spectra of B_8^- is excellent, confirming unequivocally its heptagonal structure.

The D_{8h} B_9^- has closed shell with a highly degenerate electronic configuration: $1a_{1g}^2 1e_{1u}^4\ 1e_{2g}^4 1e_{3u}^4 2a_{1g}^2 1b_{2g}^2 1a_{2u}^2$-$2e_{1u}^4 1e_{1g}^4$. Detachment from the $1e_{1g}$ HOMO results in a $^2E_{1g}$ state for B_9. The calculated VDE for this detachment channel is 3.47 eV, in excellent agreement with the measured VDE of the X band at 3.46 eV (Table 1). However, the $^2E_{1g}$ state is expected to undergo a Jahn–Teller distortion to the D_{2h} ground state of B_9 ($^2B_{1g}$). Our calculated adiabatic detachment energy (ADE) or the EA of B_9 is 3.43 eV, which is very similar to the calculated VDE and agrees well with the experimental ADE of 3.39 ± 0.06 eV. The similarity between the VDE and ADE suggests that the Jahn–Teller effect in B_9 is small, consistent with the minor geometry changes between B_9^- and B_9 (Figure 2d, e) and the sharp spectral pattern of the X band. The next detachment channel is from the $2e_{1u}$ orbital (HOMO-1) with a calculated VDE at 5.07 eV. The experimental VDE of the A band is in excellent agreement with this detachment channel. This calculated spectral pattern gives a large energy gap between 3.5 and 5 eV, which suggests that there are no single-electron transitions in this energy range. Thus, the broad X″ band may have two origins: either owing to two-electron transitions or arising from a strong Jahn–Teller splitting of the detachment from the degenerate $2e_{1u}$ HOMO-1. We suspect that both of these mechanisms may contribute to the X″ band, but at this point we are not able to definitely resolve this issue because it is challenging to calculate the Jahn–Teller distortions for the excited states. The next detachment is from

the $1a_{2u}$ orbital with a calculated VDE of 5.78 eV at the ROVGF level of theory (Table 1). The ROVGF method may have significantly underestimated the VDE because no intense detachment channels were observed between 5.08 and 6.4 eV in the PES spectrum of B_9^- (Figure 1d).

The overall excellent agreement between the predicted detachment energies and the PES spectra of B_8^- and B_9^- lend considerable credibility to the wheel structures found for B_8, B_8^-, B_8^{2-}, B_9, and B_9^-. Now the question is why these clusters adopt such unusual and beautiful structures? Insight can be gained from a detailed analysis of their valence MOs, as shown in Figure 3 for the closed shell B_8^{2-} (Figure 3a) and B_9^- (Figure 3b). For each molecule, we can identify two sets of MOs, one set responsible for the peripheral B–B bonding and the other set for bonding between the central atom and the peripheral B atoms. The latter set is the same in both molecules: the $1e_1'$, $2e_1'$, $1a_2''$, and $2a_1'$ for B_8^{2-}; $1e_{1g}$, $2e_{1u}$, $1a_{2u}$, and $2a_{1g}$ for B_9^-. To confirm this classification of the MOs, we performed a model MO calculation of a cyclic Be_8, which would have similar peripheral bonding as that in B_9^-. Indeed we found that the eight MOs of the cyclic Be_8 are very similar to the eight MOs responsible for the peripheral B–B bonding in B_9^-.

Among the six MOs responsible for the central B atom and peripheral B atom bonding, three are π orbitals ($1e_1''$ and $1a_2''$ in B_8^{2-}; $1e_{1g}$ and $1a_{2u}$ in B_9^-). These π-orbital patterns are very similar to those in the prototypical aromatic molecule, benzene. Thus, the B_8^{2-} and B_9^- molecules can be considered to be aromatic, each with six π electrons conforming to the $(4n+2)$ Hückel rule. The π aromaticity in SiB_8, which is valence isoelectronic to B_9^-, was discussed by Minyaev et al.[14] However, we believe that the B_8^{2-} and B_9^- molecules are not only π aromatic, but also σ aromatic. The three σ orbitals in each molecule ($2e_1'$ and $2a_1'$ in B_8^{2-}; $2e_{1u}$ and $2a_{1g}$ in B_9^-), which describe bonding between the central atom and the ring, are also highly delocalized and look very similar to the π MOs, thus conferring σ aromaticity on these clusters. We believe that the double aromatic characters in the chemical bonding of B_8^{2-} and B_9^- are responsible for their planarity and their unique coordination environments. When one electron is detached from B_8^{2-} or B_9^-, the π aromaticity is reduced and the Jahn–Teller effect leads to a slightly distorted B_8^- or B_9, but they are still strongly bonded systems because the σ bonding framework remains the same. When two electrons are removed from B_8^{2-}, the degenerate $1e_1''$ HOMO becomes half-filled, which resulting in the triplet B_8 ground state with very little structural change (Figure 2a and b). The triplet ground state (^3A_g) of B_8 is highly π aromatic according to the alteration of the Hückel rule for triplet states.[15,16]

To further confirm aromaticity in the molecular wheels, we calculated nucleus-independent chemical shifts (NICS)[17] for the two doubly aromatic closed-shell boron clusters: B_8^{2-} and B_9^-. In Table 2 we presented the NICS values calculated above the center of the cluster and above the B_3 triangular ring in B_8^{2-} and B_9^-. The very high NICS values (compared to benzene with NICS $= -8.0$ ppm at B3LYP6-311++G**) clearly show the presence of σ and π aromaticity in the two clusters.

Table 2: Calculated NICS in ppm at B3LYP6-311 + G* for B_8^{2-} and B_9^-.

R [Å]	NICS above the center of the cluster	NICS above the center of the B_3 ring
	B_8^{2-}	
0.5	−27.0	−35.7
1.0	−24.8	−20.8
1.5	−14.0	−11.3
2.0	−8.5	−6.9
2.5	−5.5	−4.5
3.0	−3.7	−3.1
	B_9^-	
0.5	−23.2	−33.0
1.0	−25.6	−21.0
1.5	−15.3	−12.1
2.0	−9.2	−7.3
2.5	−5.8	−4.7
3.0	−3.8	−3.1

The chemical bonding between the central boron and the ring can be viewed as spokes of the molecular wheels. However, the delocalized nature of MOs describing the center-to-ring bonding suggests that individual spokes cannot be identified, much like a bicycle wheel spinning at a high speed. Hence, instead of spokes, the molecular wheels are strengthened by a "disk". Recently, two aromatic planar pentacoordinate iron cations ($[FeSb_5]^+$ and $[FeBi_5]^+$) have been predicted,[18] which exhibit similar delocalized bonding between the central Fe and the Sb_5 or Bi_5 ring. This is an unprecedented delocalization pattern, which is different from the familiar cyclic delocalization in benzene. It may be appropriate to call this delocalization in the molecular wheels "disk delocalization".

Tetracoordinate planar carbon was proposed 30 years ago by Hoffmann et al.[19] and has been confirmed experimentally.[20,21] More highly coordinated planar carbon and other main-group atoms have been proposed.[13, 14] Our work is the first confirmation of hepta- and octacoordinated boron atoms and demonstrates that σ and π aromaticity are responsible for the highly unusual coordination environments. It should be emphasized that detailed understanding of novel molecular structures using concepts of chemistry will be increasingly important in nanotechnology as device features rapidly approach the atomic and molecular scale.

Methods

Photoelectron Spectroscopy: Details of the experimental apparatus have been published elsewhere.[22,23] Briefly, a compressed disk made with pure ${}^{10}B$ isotope (98% enriched) was used as the laser vaporization target with helium carrier gas. Clusters from the source underwent a supersonic expansion and collimated with a skimmer. Negatively charged clusters were extracted from the cluster beam and were analyzed by a time-of-flight (TOF) mass spectrometer. The B_8^- and B_9^- cluster ions were mass-selected before photodetachment with one of the three photon energies: 355 nm (3.496 eV), 266 nm (4.661 eV), and 193 nm (6.424 eV). The use of a single isotope target greatly simplified the mass spectra and allowed clean mass selections without any contamination. Photoelectron spectra were measured using a magnetic-bottle TOF photoelectron

analyzer with an electron kinetic energy resolution of $\Delta E_k/E_k \approx 2.5\%$. The spectrometer was calibrated with the known spectrum of Rh^-.

Theoretical Calculations: Theoretical methods used in this work were described in more detail elsewhere.[4,5] The initial search for the global minima of B_8, B_8^-, B_9, and B_9^- and vibrational frequency calculations were performed using analytical gradients with polarized split-valence basis sets (6-311 + G*) and the hybrid method, known as B3LYP. Some geometries and vibrational frequencies were further refined with the multiconfigurational method CASSCF with various active spaces. The coupled-cluster method [CCSD(T)] with 6-311 + G* basis set was used for additional geometry optimizations, and for refinement of energies with the 6-311 + G(2df) and 6-311 + G(2d) basis sets. Vertical electron detachment energies were calculated using the restricted and unrestricted coupled-cluster methods R(U)CCSD(T)/6-311 + G(2df), at the equation-of-motion method based on RCCSD(T) [EOM-RCCSD(T)] with the same 6-311 + G(2df) basis set and at the outer-valence Green Function method (ROVGF). Molecular orbitals were calculated at the U(R)HF/6-311 + G* levels of theory. U(R)HF, B3LYP, CASSCF, ROVGF, and CCSD(T) calculations were performed using Gaussian 98.[24] RCCSD(T) and EOM-RCCSD(T) calculations—using MOLPRO 1999 program.[25] Molecular orbital pictures were made using MOLDEN3.4 program.[26] All calculations were performed on a 63-nodes Birch-Retford Beowulf cluster computer built at Utah State by K. A. Birch and B. P. Retford.

[1] W. L. Lipscomb, *Boron Hydrides*, W. A. Benjamin, New York, **1963**.
[2] *Boron Hydride Chemistry* (Ed.: E. L. Meutterties), Academic Press, New York, **1975**.
[3] F. A. Cotton, G. Wilkinson, C. A. Murillo, M. Bochmann, *Advanced Inorganic Chemistry*, 6th ed., Wiley, New York, **1999**.
[4] H. J. Zhai, L. S. Wang, A. N. Alexandrova, A. I. Boldyrev, *J. Chem. Phys.* **2002**, *117*, 7917.
[5] A. N. Alexandrova, A. I. Boldyrev, H. J. Zhai, L. S. Wang, E. Steiner, P. W. Fowler, *J. Phys. Chem. A* **2003**, *107*, 1359.
[6] X. Li, A. E. Kuznetsov, H. F. Zhang, A. I. Boldyrev, L. S. Wang, *Science* **2001**, *291*, 859.
[7] A. I. Boldyrev, L. S. Wang, *J. Phys. Chem. A* **2001**, *105*, 10759.
[8] J. Li, X. Li, H. J. Zhai, L. S. Wang. *Science* **2003**, *299*, 864.
[9] V. Bonacic-Koutecky, P. Fantucci, J. Koutecky, *Chem. Rev.* **1991**, *91*, 1035.
[10] H. Kato, K. Yamashita, K. Morokuma, *Chem. Phys. Lett.* **1992**, *190*, 361.
[11] A. K. Ray, I. A. Howard, K. M. Kanal, *Phys. Rev. B* **1992**, *45*, 14247.
[12] I. Boustani, *Phys. Rev. B* **1997**, *55*, 16426.
[13] Z. X. Wang, P. von R. Schleyer, *Science* **2001**, *292*, 2465.
[14] R. M. Minyaev, T. N. Gribanova, A. G. Starikov, V. I. Minkin, *Mendeleev Commun.* **2001**, 1–2.
[15] N. C. Baird, *J. Am. Chem. Soc.* **1972**, *94*, 4941.
[16] V. I. Minkin, M. N. Glukhovtsev, B. Y. Simkin, *Aromaticity and Antiaromaticity*, Wiley, New York, **1994**.
[17] P. von R. Schleyer, C. Maerker, A. Dransfeld, H. Jiao, N. J. R. v. E. Hommes, *J. Am. Chem. Soc.* **1996**, *118*, 6317.
[18] M. Lein, J. Frunzke, G. Frenking, *Angew. Chem.* **2003**, *115*, 1341; *Angew. Chem. Int. Ed.* **2003**, *42*, 1303.
[19] R. Hoffmann, R. W. Alder, C. F. Wilcox, Jr., *J. Am. Chem. Soc.* **1970**, *92*, 4992.

[20] D. Rottger, G. Erker, *Angew. Chem.* **1997**, *109*, 840; *Angew. Chem. Int. Ed.* **1997**, *36*, 812.

[21] L. S. Wang, A. I. Boldyrev, X. Li, J. Simons, *J. Am. Chem. Soc.* **2000**, *122*, 7681.

[22] L. S. Wang, H. Wu in *Advances in Metal and Semiconductor Clusters. IV. Cluster Materials* (Ed.: M. A. Duncan), JAI, Greenwich, CT, **1998**, pp. 299 – 343.

[23] L. S. Wang, X. Li in *Clusters and Nanostructure Interfaces* (Eds.:P. Jena, S. N. Khanna, B. K. Rao), World Scientific, New Jersey, **2000**, pp. 293 – 300.

[24] Gaussian 98 (Revision A.7), M. J. Frisch, G. W. Trucks, H. B. Schlegel, G. E. Scuseria, M. A. Robb, J. R. Cheeseman, V. G. Zakrzewski, J. A. Montgomery, R. E. Stratmann, J. C. Burant, S. Dapprich, J. M. Millam, A. D. Daniels, K. N. Kudin, M. C. Strain, O. Farkas, J. Tomasi, V. Barone, M. Cossi, R. Cammi, B. Mennucci, C. Pomelli, C. Adamo, S. Clifford, J. Ochterski, G. A. Petersson, P. Y. Ayala, Q. Cui, K. Morokuma, D. K. Malick, A. D. Rabuck, K. Raghavachari, J. B. Foresman, J. Cioslowski, J. V. Ortiz, B. B. Stefanov, G. Liu, A. Liashenko, P. Piskorz, I. Komaromi, R. Gomperts, R. L. Martin, D. J. Fox, T. Keith, M. A. Al-Laham, C. Y. Peng, A. Nanayakkara, C. Gonzalez, M. Challacombe, P. M. W. Gill, B. G. Johnson, W. Chen, M. W. Wong, J. L. Andres, M. Head-Gordon, E. S. Replogle, J. A. Pople, Gaussian, Inc., Pittsburgh, PA, **1998**.

[25] MOLPRO 1999 program is by J. H. Werner, P. J. Knowles with contributions from R. D. Amos, A. Bernhardsson, A. Berning, P. Celani, D. L. Cooper, M. J. O. Deegan, A. J. Dobbyn, F. Eckert, C. Hampel, G. Hetzer, T. Korona, R. Lindh, A. W. Llpyd, S. J. McNicholas, F. R. Manby, W. Meyer, M. E. Mura, A. Nicklass, P. Palmieri, R. Pitzer, G. Rauhut, M. Schutz, H. Stoll, A. J. Stone, R. Tarroni, T. Thorsteinsson.

[26] G. Schaftenaar, MOLDEN3.4, CAOS/CAMM Center, The Netherlands, **1998**.